Fast H-Waves in Double Comb Infinite Arrays

Alexander Ye. Svezhentsev[1, *],
Vladimir S. Miroshnichenko[1], and Guy A. E. Vandenbosch[2]

Abstract—A rigorous approach to study the fast H-waves which propagate across an infinite double comb array (IDCA) is proposed. It is based on the Floquet theorem combined with the advanced moment method (Galerkin) scheme in which the basis explicitly satisfies the edge conditions at the rectangular wedge. An exhaustive analysis of the regular and singular modes of the IDCA is made. Normalized critical wave numbers and modal fields are investigated in terms of geometrical parameters. Coupling effects between different IDCA modes are found. For the singular modes a new analytical formula for the critical normalized wave numbers is obtained.

1. INTRODUCTION

Mastering the low and sub mm range remains a vital strategy in vacuum electronics. This concerns classical electronic devices like travelling wave tube amplifiers, backward wave oscillators, diffraction radiation oscillators, reflex klystrons, etc. [1–10]. These devices use different principles of interaction between the electron beam and electromagnetic waves.

In devices like the travelling wave tube amplifier the slow wave propagating along a comb periodical structure is used. However, other regimes of the comb periodical structure may occur. In particular, in a diffraction radiation oscillator (DRO) [7–10] fast H-waves propagate across the comb periodical structure. In this case the angle between the wave direction and the electron beam is 90°. To provide the DRO with a high Q-factor and to ensure an effective energy exchange between the electron beam and the open resonator field, the knowledge of the exact critical wave numbers and the field structure of the H-wave propagating across the double comb periodical structure is crucial [10].

In this paper, for the first time, the fast H-wave propagating in a double comb array (DCA) is analyzed. First, the large finite DCA is approximated by an infinite array (ICDA). Second, the periodical structure is solved with a method of moments procedure. A combination of the Floquet theorem and the Galerkin scheme is used. The basis functions explicitly satisfy the edge conditions at the rectangular wedge. The so-called Sub Domain Edge (SDE) method is used. This technique is faster and much more stable than pure numerical solutions like FEM or FDTD. The SDE method was already applied to study wave propagation in complex shape waveguides, slot and strip lines, and groove waveguides [11, 12]. The method was extended to study waves in single infinite periodic arrays with a groove of complex cross section [13]. Recently it was used to study slow waves along a double comb array placed in a rectangular waveguide [14].

The principal mode of the IDCA was very preliminary studied in [15]. In this paper, an exhaustive analysis of the IDCA is given, not only of the principal H-mode but also of the higher order H-modes. The analysis is performed in terms of geometrical parameters, full field distributions are studied, and new coupling effects are found. It is shown that the modal spectrum contains both regular and singular waves.

2. PROBLEM FORMULATION AND SOLUTION

Consider the IDCA in Fig. 1(a), H-waves that propagate in z-direction have a dependence on z and time given by $e^{-i(hz-\omega t)}$, where h is the propagation constant and ω the angular frequency. Since the structure is periodic with period L the analysis of the whole structure is reduced to the analysis of a single unit cell, see Fig. 1(b). Taking into account the symmetry, electric and magnetic walls can be applied in the symmetry planes (see dotted lines OB and BC). The dimensions are defined as OF = AE = c, AB = g, BC = $L/2$, OA = b, OB = $a/2 = g + b$. Within the unit cell we introduce two subdomains: $g < x < g + b$, $0 < y < c$ (1) and $0 < x < g$, $0 < y < L/2$ (2). The selection of electric or magnetic wall boundaries is defined as follows:

- wall BC: electric wall corresponds to $g1 = 0$, magnetic to $g1 = 1$,
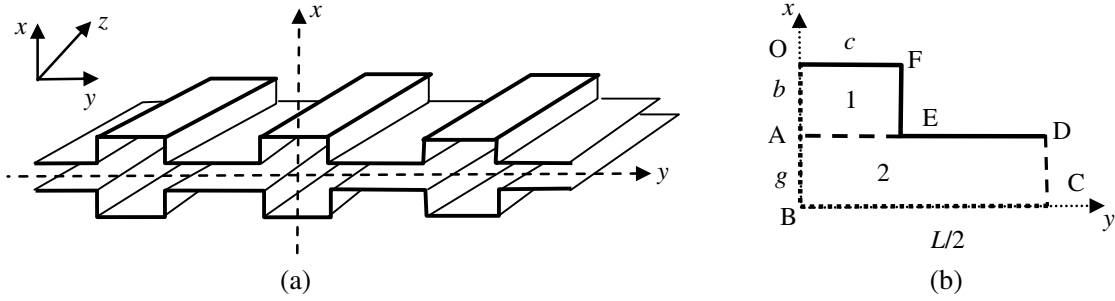- wall OB: electric wall corresponds to $g2 = 0$, magnetic to $g2 = 1$.

(a)   (b)

Figure 1. The IDCA: (a) isometric and (b) cross-sectional view of unit cell.

The critical wave numbers k_c of the H-wave ($H_z \neq 0$, $E_z = 0$) of the IDCA are found by solving the two-dimensional Helmholtz equation

$$\frac{d^2 H_{(1,2),z}}{dx^2} + \frac{d^2 H_{(1,2),z}}{dy^2} + k_c^2 \cdot H_{(1,2),z} = 0, \tag{1}$$

where k_0 and k_c are the free space and critical wave numbers and $k_c^2 = k_0^2 - h^2$.

The solution of Eq. (1) in regions 1 and 2 can be presented as a series in eigenfunctions of domains 1 and 2 (taking into account the Floquet theorem) with the coefficients unknown:

$$H_{1,z}(x,y) = \sum_{n=0}^{\infty} A_n X_{1n}(x) Y_{1n}(y), \tag{2}$$

$$H_{2,z}(x,y) = \sum_{n=0}^{\infty} B_n X_{2n}(x) Y_{2n}(y), \tag{3}$$

where $H_{(1,2),z}(x,y)$ is the z-component of the magnetic field, and A_n, B_n are unknown coefficients,

$$X_{1n}(x) = \cos\left[p_n(x - g - b)\right], \quad X_{2n}(x) = \sin\left[\chi_n x - \pi g_1/2\right] \tag{4}$$
$$Y_{1n}(y) = \mu_{1n} \cos\left[\alpha_n y - \pi g_2/2)\right], \quad Y_{2n}(y) = \mu_{2n} \cos\left[\Delta_n y - \pi g_2/2\right] \tag{5}$$

with

$$\alpha_n = \pi(n + g_2/2)/c, \quad \Delta_n = 2\pi n/L, \quad p_n^2 = k_c^2 - \alpha_n^2, \quad \chi_n^2 = k_c^2 - \Delta_n^2, \quad \mu_{1n} = \sqrt{(2 - \delta_{0\alpha_n})/c}, \tag{6}$$

$$\delta_{0\alpha_n} = \begin{cases} 1, & \text{if } \alpha_n = 0 \\ 0, & \text{if } \alpha_n \neq 0 \end{cases}, \quad \mu_{2n} = \sqrt{2/L}, \quad k_0 = 2\pi/\lambda_0, \quad k_c = 2\pi/\lambda_c, \tag{7}$$

and λ_0, λ_c the free space and critical wavelengths, respectively.

Note that the functions $X_{in}(x)$, $Y_{in}(y)$ already satisfy the boundary conditions. The functions $Y_{1n}(y)$ and $Y_{2n}(y)$ form complete bases over the segments $[0,\ c]$ and $[0,\ L/2]$, respectively. These

functions are normalized by the coefficients μ_{1n} and μ_{2n}, respectively. Quantities p_n and χ_n can be obtained by substituting Eqs. (4)–(5) into the Helmholtz equation (1) for the H_z components.

The formulas in (2)–(3) are different from the corresponding formulas in [15] since they explicitly take into account the electric or magnetic walls in the symmetry planes (see Fig. 1(b)), resulting in Eq. (3) in a summation from 0 to ∞, instead of $-\infty$, ∞ in [15]. These electric and/or magnetic walls considerably reduce the order of the resulting system of equations and, more importantly, they allow to split the solution into four independent ones. This is crucial for the categorization of all possible field solutions and opened the way to a detailed study of the IDCA mode spectrum, including the observation of the physical peculiarities discussed later.

The first step in obtaining the integral equation consists of satisfying the boundary conditions which are continuity conditions at $x = g$, $0 < y < c$. Applying the continuity condition for the electric field y-component

$$E_{1,y} = E_{2,y} = f(y) \tag{8}$$

at $x = g$, $0 < y < c$ we can express the unknown coefficients A_n and B_n via the unknown function $f(y)$. Doing the same for the magnetic field z-component we come to the integral equation

$$\tilde{D}f = \int_o^c f(y) \left\{ \sum_{n=0}^{\infty} \left[F_{1n} X_{1n}(g) Y_{1n}(y) Y_{1n}(y') - F_{2n} X_{2n}(g) Y_{2n}(y) Y_{2n}(y') \right] \right\} dy = 0, \tag{9}$$

where

$$F_{1n}(y) = 1/X'_{1n}(g), \quad F_{2n}(y) = 1/X'_{2n}(g). \tag{10}$$

The integral equation (9) is solved using Galerkin's scheme with basis functions that explicitly satisfy the edge condition. The solution can be expressed in the form:

$$f(y) = \sum_{i=0}^{NR-1} U_i \Phi_i(y), \tag{11}$$

where U_i are unknown coefficients, NR is the number of basis functions, and

$$\Phi_i(y) = \sigma^{-1}(y)\varphi_i(y); \quad \sigma(y) = \left[1 - (y/c)^2 \right]^{1/3}; \quad \varphi_i(y) = C_{2i+g_2}^{1/6}(y/c) \tag{12}$$

In Eqs. (11)–(12) $\sigma(y)$ is the weight function that gives the correct edge behavior near the rectangular edge and $\varphi_i(y)$ is a Gegenbauer polynomial [16]. The functions $\varphi_i(y) = C_{2i+g_2}^{1/6}(y/c)$ form a complete basis over the segment $[0, c]$ with the weigh function $\sigma(y)$. Note that the parameter g_2 enters into formula (12c) due to the fact that the type of wall at the OB boundary sets the corresponding behavior (evenness/oddness) for the E_y component with respect to the $y = 0$ plane (see Fig. 1(b)). Realizing the Galerkin scheme we come to a system of linear algebraic equations for the unknown coefficients U_i:

$$\sum_{i=0}^{NR-1} U_i D_{ij} = 0, \quad i,j = 0,1,\ldots,NR-1, \tag{13}$$

where

$$D_{ij} = \int_0^c \Phi_i(y') \tilde{D}[\Phi_j(y)] dy' = \sum_{n=0}^{\infty} \left\{ F_{1n} X_{1n}(g) \psi_{in}(\alpha_n) \psi_{jn}(\alpha_n) - F_{2n} X_{2n}(g) \psi_{in}(\Delta_n) \psi_{jn}(\Delta_n) \right\}, \tag{14}$$

$$\psi_{(i,j)n}(\alpha_n) = \int_0^c \Phi_{(i,j)}(y) Y_{1n}(y) dy, \quad \psi_{(i,j)n}(\Delta_n) = \int_0^c \Phi_{(i,j)}(y) Y_{2n}(y) dy. \tag{15}$$

Note that integrals in Eq. (15) are explicitly calculated via Bessel functions with non integer index [11, 13, 16]. The resulting dispersion equation has a form:

$$\det\left[D_{ij}\right] = 0, \quad i,j = 0,1,2,\ldots,NR-1, \tag{16}$$

where matrix elements $D_{i,j}$ can be expressed as:

$$D_{i,j} = \sum_{n=0}^{\infty} \left\{ (\mu_{1n})^2 \bar{F}_{1n} W_i(\alpha_n c) W_j(\alpha_n c) - (\mu_{2n})^2 \bar{F}_{2n} W_i(\Delta_n c) W_j(\Delta_n c) \right\} \qquad (17)$$

with

$$W_i(\alpha_n c) = J_{2i+1/6+g_2}(\alpha_n c)/(\alpha_n c)^{1/6}, \quad W_i(\Delta_n c) = J_{2i+1/6+g_2}(\Delta_n c)/(\Delta_n c)^{1/6}, \qquad (18)$$

$$\bar{F}_{1n} = \cos(p_n b)/(p_n \sin(p_n b)), \quad \bar{F}_{2n} = -\cos(\bar{\chi}_n g)/(\bar{\chi}_n \sin(\bar{\chi}_n g)), \quad \bar{\chi}_n = \chi_n - \pi g_1/2, \quad (19)$$

where $J_\nu(z)$ is a Bessel function. Note that the parameter g_2 enters into the index of the Bessel function (see Eq. (18)) while the parameter g_1 enters into the arguments of the trigonometric functions in Eq. (19).

Thus we obtain the dispersion Equation (16) which incorporates four different $(g1/g2)$ pair values. It is this fact that allows categorizing the solution into four independent families.

Equation (16) can be solved by Newton's method to find the critical wave numbers k_c. Due to the fact that the topology is closed k_c has to be real. It was numerically found that in order to get a stable solution for k_c with three significant digits, it is sufficient to perform the summations over about three hundred terms and to take the reduction order of Eq. (16) as $NR = 4$, equal to the number of basis functions. The boundary conditions at the boundary between subdomains 1 and 2 are then satisfied with an accuracy of about 0.1% far from the edge and about 2% near the edge.

The set of H-waves can be subdivided into four different families according to the symmetry planes, as discussed in detail in Section 4.

3. H-WAVES SPECTRUM

The IDCA cell geometry evolution versus g/a is shown in Fig. 2. First a qualitative analysis of the IDCA spectrum is given. Classification of the waves within the IDCA is not trivial because the IDCA spectrum in the cases $g/a \to 0$ and $g/a \to 0.5$ (see Fig. 2) cannot be fully reduced to the spectrum of H-waves within traditional rectangular ($g/a = 0$) and plane ($g/a = 0.5$) waveguides (see Fig. 2), respectively. In the cases $g/a \to 0$ and $g/a \to 0.5$ (see Fig. 2) there are new wave types, as will be shown below, which do not occur in the spectrum at $g/a = 0$ and $g/a = 0.5$ (see Fig. 2), respectively. For $0 < g/a < 0.5$ these additional waves appear as a consequence of the periodicity. The IDCA spectrum thus consists of regular and singular waves, where the singular waves will disappear at the extremes for $g/a = 0$ and $g/a = 0.5$ (see Fig. 2).
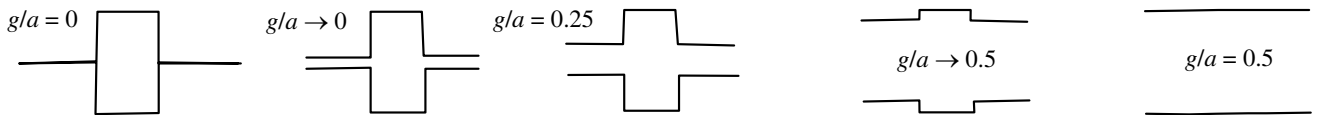

Figure 2. Cell evolution versus g/a.

It is obvious that at $g/a = 0$ the IDCA spectrum consists of the regular $H_{mn}^{g1,g2}$ ($m, n = 0, 1, \ldots$) waves of the rectangular waveguide and that at $g/a = 0.5$ the IDCA spectrum consists of the regular $H_p^{g1,g2}$ ($p = 0, 1, \ldots$) waves of the plane waveguide. These waves continue to exist for any g within the range $0 < g/a < 0.5$. For $g/a \to 0$ (see Fig. 2) the waves of the singular array type $XH_{ms}^{g1,g2}$ ($m, s = 0, 1, \ldots$) appear and exist further for all $0 < g/a < 0.5$ values. Similarly, for $g/a \to 0.5$ the singular waves of the array type $XH_{ps}^{g1,g2}$ ($p, s = 0, 1, \ldots$) appear and exist further for all $0 < g/a < 0.5$ values. The indices m and p represent the number of half wavelengths in the x direction for the double cell, i.e., taking into account the symmetry plane at BC with the corresponding wall (see Fig. 1(b)). The indices n (used further) and s represent the number of half wavelengths in the y direction in the regions 1 and 2, respectively, for the double cell, i.e., taking into account the symmetry plane at OB with the corresponding wall. It is reasonable to assume that the critical wave numbers of the regular and singular waves are continuously transforming when the parameter g/a varies from $g/a \to 0$ to $g/a \to 0.5$

(see Fig. 2). For this transformation (or transition) we will use the symbol "↔". For example, writing $H_{40}^{0,0} \leftrightarrow XH_{01}^{0,0}$ means that the normalized critical wave number of the regular $H_{40}^{0,0}$ $(g/a = 0)$ wave is continuously transforming to the normalized critical wave number of the $XH_{01}^{0,0}$ $(g/a \to 0.5)$ wave when g/a continuously varies from $g/a = 0$ to $g/a \to 0.5$ ($g1$ and $g2$ are both equal to zero).

The quantitative analysis of the IDCA spectrum is based on applying the limits $g/a \to 0$ and $g/a \to 0.5$ (see Fig. 2) to the formulas (4), respectively. Inserting the extreme case $g/a = 0$ we obtain the $H_{mn}^{g1,g2}$ waves of the rectangular waveguide with normalized critical wave numbers $k_c a = \pi\sqrt{m^2 + (n/(2c/a))^2}$, where $m = 2k + g_1$, $n = 2q + g_2$, $k = 0, 1, \ldots$, $q = 0, 1, \ldots$.

As mentioned above the singular $XH_{ms}^{g1,g2} \leftrightarrow XH_{ps}^{g1,g2}$ waves exist in the structure for any $0 < g/a < 0.5$ but not in the extreme cases $g/a = 0$ and $g/a = 0.5$. Analytical formulas for the $XH_{ps}^{g1,g2}$ critical wave numbers can be obtained in the case $g/a \to 0.5$ (see Fig. 2). Inserting this limit into formula (4b) we obtain

$$k_c a = \pi\sqrt{p^2 + 4(s/(L/a))^2}, \tag{20}$$

where $p = 2k + g_1$, $k = 0, 1, \ldots$, and $s = 0, 1, \ldots$. Note that the parameter g_2 does not enter into the index s because the region 2 (see Fig. 1(b)) does not contain a side wall at the CD position. This means that the same s value can occur in different families with corresponding wall in the $y = 0$ plane. It is seen that the waves continuously transform, i.e., $XH_{ms}^{g1,g2} \leftrightarrow XH_{ps}^{g1,g2}$, when the parameter g/a varies. This means that the index m can transform to p due to the mode coupling, as will be studied below. Also note that the formula (20) is an approximation obtained in the case $g/a \to 0.5$ and in this approximation the critical wave number does not depend on the groove geometry.

The value $s = 0$ in Eq. (20) corresponds to the $H_p^{g1,g2}$ waves of the plane waveguide ($g/a = 0.5$, see Fig. 2) with normalized critical wave numbers $k_c a = \pi p$, where $p = 2k + g_1$, $k = 0, 1, \ldots$.

Summarizing, the possible wave transformations that can take place in the IDCA in the range $0 \le g/a \le 0.5$ are: $H_{mn}^{g1,g2} \leftrightarrow H_p^{g1,g2}$ ($m, p = 0, 1, \ldots$, $n = 0, 1, \ldots$) for the regular waves, $XH_{ms}^{g1,g2} \leftrightarrow XH_{ps}^{g1,g2}$ for the singular waves, $H_{mn}^{g1,g2} \leftrightarrow XH_{ps}^{g1,g2}$ for regular $\leftrightarrow$ singular, $XH_{ms}^{g1,g2} \leftrightarrow H_p^{g1,g2}$ for singular $\leftrightarrow$ regular. The regular waves $H_{mn}^{g1,g2}$ always exist at both $g/a = 0$ and for $g/a \to 0$, the regular waves $H_p^{g1,g2}$ always exist for both $g/a \to 0.5$ and $g/a = 0.5$, while the singular waves $XH_{ms}^{g1,g2}$, $XH_{ps}^{g1,g2}$ do not exist at the exact points $g/a = 0$ and $g/a = 0.5$, respectively.

4. NUMERICAL RESULTS

In case of the _family H_z-odd $(g_1 = 1)$/H_z-even $(g_2 = 0)$_ there is a magnetic wall at BC and an electric wall at OB (see Fig. 1(b)). The IDCA is configured with $c/a = 0.0484$, $L/a = 0.3876$, $L/(2c) = 4.004$. Fig. 3, a shows the transitions of the waves $H_{mn}^{g1,g2}$ into $H_m^{g1,g2}$ and $XH_{ps}^{g1,g2}$ waves versus the parameter g/a. Note that at $g/a \to 0.5$ next to the regular waves there are two singular waves: $XH_{11}^{1,0}$ and $XH_{31}^{1,0}$ which do not belong to the set of waves of the plane waveguide because they are not present at $g/a = 0.5$. As seen from Fig. 3, a there is a good agreement for the lowest $H_{10}^{1,0} \leftrightarrow H_1^{1,0}$ wave (see curve 1) between the proposed SDE solution (solid line 1) and calculations with the commercial solver CST Microwave Studio (rectangular dots). The distribution of the H_z-component for the principal $H_{10}^{1,0} \leftrightarrow H_1^{1,0}$ wave in the cross-section is given in Fig. 3(b). Note that the lines $H_z = $ const coincide with the force lines of the electrical field. A schematic view of the transversal electric and magnetic field structure of the $H_{10}^{1,0} \leftrightarrow H_1^{1,0}$ wave is presented in Fig. 3(c). As an example of the field transition Figs. 4(a), (b) give the H_z-component distribution for the wave $H_{70}^{1,0} \leftrightarrow XH_{11}^{1,0}$ in both extreme cases: $g/a = 0.01$ and $g/a = 0.49$ (see curve 4 in Fig. 3(a)). Note that the wave $XH_{11}^{1,0}$ does not exist at $g/a = 0.5$.

It is observed in Fig. 3 that curves 3 and 4 approach each other and then recede from each other. The corresponding region is marked by a circle. This effect is known as the modes mutual coupling phenomenon. This effect was observed already for modes in open resonators [17], for slow waves in cylindrical [18] and planar [19] slot and strip lines, and in open waveguides of complex cross-section [13]. The plots in Fig. 3, a reveal a lot of such coupling effects. Note that in the coupling region the Morse critical point is observed [13, 17–19]. A qualitative picture of the mutual coupling phenomenon in the
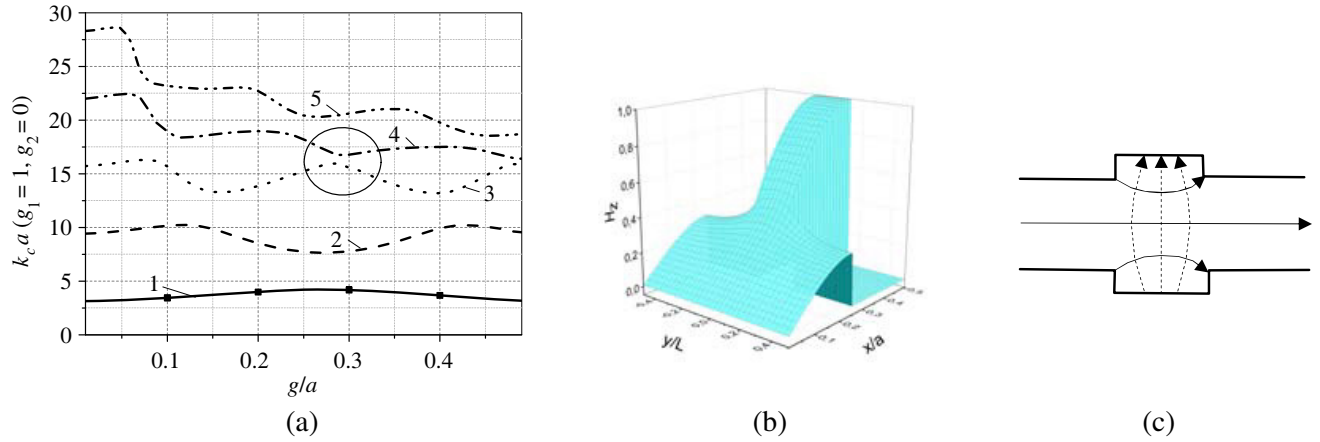
(a)   (b)   (c)

Figure 3. (a) Normalized critical wave number $k_c a$ versus g/a. $c/a = 0.0484$, $L/a = 0.3876$, $L/(2c) = 4.004$. The waves transition are: 1 — $H_{10}^{1,0} \leftrightarrow H_1^{1,0}$ (solid — SDE method, rectangles (4 dots) — CST), 2 — $H_{30}^{1,0} \leftrightarrow H_3^{1,0}$, 3 — $H_{50}^{1,0} \leftrightarrow H_5^{1,0}$, 4 — $H_{70}^{1,0} \leftrightarrow XH_{11}^{1,0}$, 5 — $H_{90}^{1,0} \leftrightarrow XH_{31}^{1,0}$. (b) — lines of $H_z = \text{const}$ for the $H_{10}^{1,0} \leftrightarrow H_1^{1,0}$ wave. $g/a = 0.25$, $c/a = 0.0484$, $L/a = 0.3876$, $L/(2c) = 4.004$. (c) transversal field structure of the dominant $H_{10}^{1,0} \leftrightarrow H_1^{1,0}$-wave. E-field in solid line, H-field in dashed line.

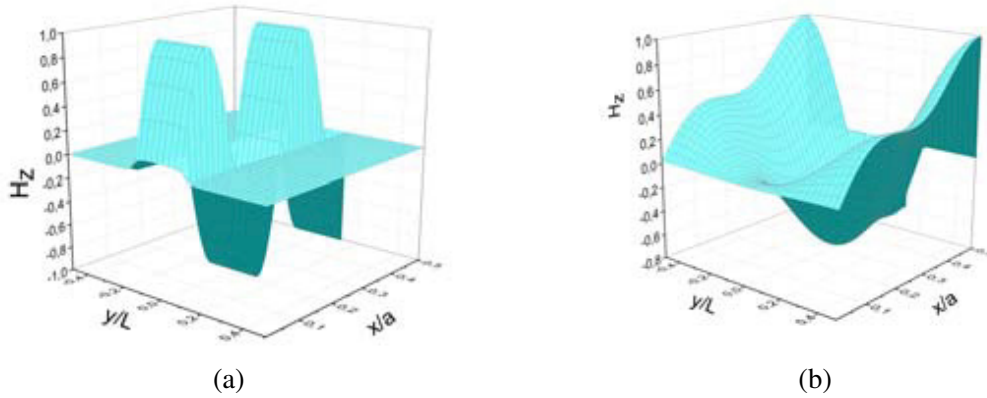(a)   (b)

Figure 4. Field transformation (H_z-component) $H_{70}^{1,0} \leftrightarrow XH_{11}^{1,0}$ (curve 4, Fig. 2); $c/a = 0.0484$, $L/a = 0.3876$, $L/(2c) = 4.004$; (a) $g/a = 0.01$, (b) $g/a = 0.49$.
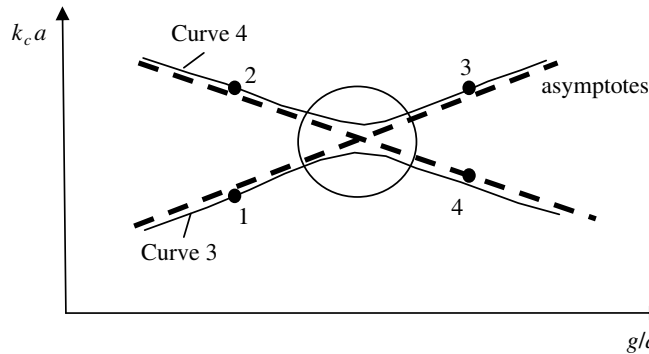

Figure 5. Schematic qualitative picture of the mutual coupling phenomenon.

coupling region of Fig. 3, a is depicted in Fig. 5. The curves 3 and 4 describe the normalized critical wave number behavior versus g/a. Formally, the points 1 and 4 belong to the same curve 3 and the points 2 and 3 belong to the same curve 4. However, the field distributions in the points 1 and 3 are similar and the field distributions in the points 2 and 4 are similar. Results which confirm the mode coupling effect are presented in Fig. 6. The field profiles depicted in Fig. 6(a) and Fig. 6(b) correspond to the same curve 4 of Fig. 3(a) and the field profiles depicted in Fig. 6(c) and Fig. 6(d) correspond to the same curve 3 of Fig. 3(a). It is seen that the field profiles in Fig. 6(a) and Fig. 6(d) are similar. The same is observed in Fig. 6(c) and Fig. 6(b).
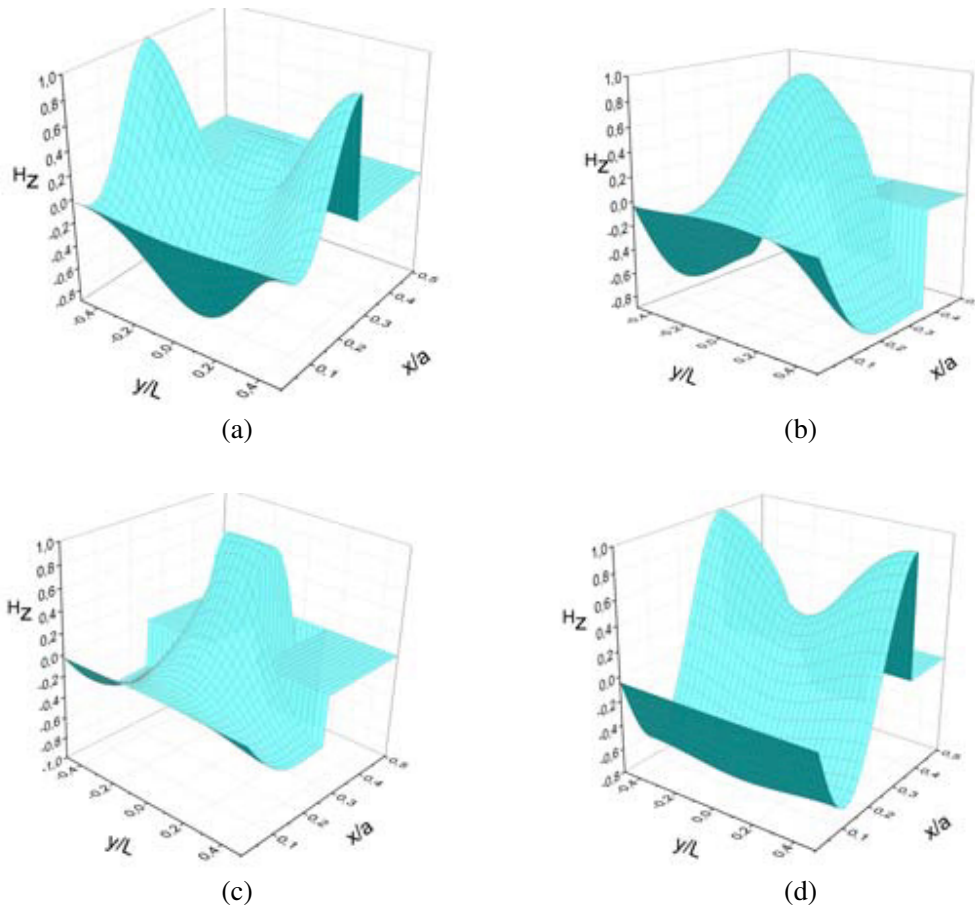

(a)

(b)

(c)

(d)

Figure 6. Mode coupling in the IDCA. The field structure (H_z-component) for curves 3–4 (see Fig. 2), $c/a = 0.0484$, $L/a = 0.3876$. (a) $g/a = 0.25$, $k_c a = 18.2241$. (b) $g/a = 0.35$, $k_c a = 17.3363$. (c) $g/a = 0.25$, $k_c a = 15.2497$. (d) $g/a = 0.35$, $k_c a = 13.9867$.

Note that a specific mode can show a coupling effect several times while g/a varies. This explains the need for different indexes (mn, ms, p, ps) in the extreme cases: in the rectangular waveguide (at $g/a = 0$ for the regular waves $H_{mn}^{g1,g2}$ and for $g/a \to 0$ for the singular waves $XH_{ms}^{g1,g2}$) and in the plane waveguide (at $g/a = 0.5$ for regular waves $H_p^{g1,g2}$ and for $g/a \to 0.5$ for the singular waves $XH_{ps}^{g1,g2}$).

The results for the *family H_z-even $(g_1 = 0)$/H_z-odd $(g_2 = 1)$* versus g/a are given in Fig. 7(a). The lowest wave in Fig. 7(a) is the singular wave $XH_{01}^{0,1} \leftrightarrow XH_{01}^{0,1}$ which holds its indexes over the whole range $0 < g/a < 0.5$. The field structure of the H_z-component and the schematic transversal field structure of this wave are shown in Fig. 7(b) and Fig. 7(c), respectively. It is interesting to note that the H_z field of the $XH_{01}^{0,1} \leftrightarrow XH_{01}^{0,1}$ wave in Fig. 7(b) is mostly concentrated in region 2. When $g/a \to 0.5$ the normalized critical number given by Eq. (20) with $p = 0$, $s = 1$ leads to
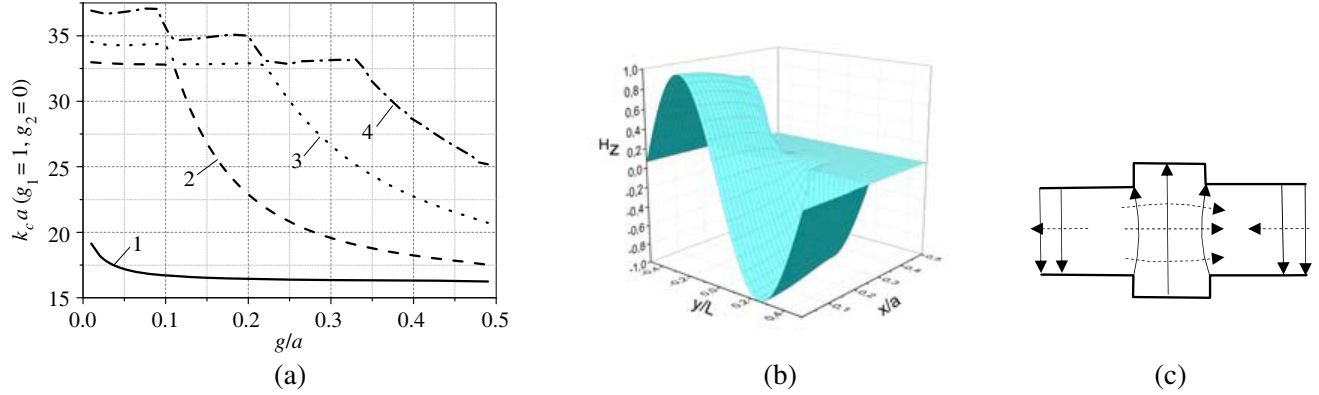
$$k_c a = 2\pi/(L/a) \Rightarrow \lambda_c = L. \tag{21}$$

Figure 7. (a) Normalized critical wave number $k_c a$ of the IDCA versus g/a. $c/a = 0.0484$, $L/a = 0.3876$, $L/(2c) = 4.004$. The wave transitions: 1 — $XH_{01}^{0,1} \leftrightarrow XH_{01}^{0,1}$, 2 — $H_{21}^{0,1} \leftrightarrow XH_{21}^{0,1}$, 3 — $H_{41}^{0,1} \leftrightarrow XH_{41}^{0,1}$, 4 — $H_{61}^{0,1} \leftrightarrow XH_{61}^{0,1}$. (b) The field structure (H_z-component) of the $XH_{01}^{0,1} \leftrightarrow XH_{01}^{0,1}$ wave. $g/a = 0.25$. $c/a = 0.0484$, $L/a = 0.3876$, $L/(2c) = 4.004$. (c) Transversal field structure of dominant $XH_{01}^{0,1} \leftrightarrow XH_{01}^{0,1}$-wave. The E-field is shown in solid line, the H-field in dashed line.

Note that curve 1 in Fig. 7(a) for $g/a \to 0.5$ tends to the value determined by Eq. (21). It is seen from Eq. (21) that the normalized critical wave number of the $XH_{01}^{0,1} \leftrightarrow XH_{01}^{0,1}$ wave for $g/a \to 0.5$ depends on L/a only. Its value in case $L/a > 2$ can be even smaller than the normalized critical wave number of the $H_{10}^{0,1} \leftrightarrow H_1^{0,1}$ wave, which is equal to π.

Thus the critical wavelength of the lowest singular wave $XH_{01}^{0,1} \leftrightarrow XH_{01}^{0,1}$ in the case $g/a \to 0.5$ is equal to the structure period L, and in the case $L > 2a$ the critical wavelength is bigger than $2a$. Formula (21) is a fundamental result. Since Eq. (21) does not contain any groove parameter, the lowest singular wave exists in the IDCA even with grooves of arbitrary shape.

For the $XH_{01}^{0,1} \leftrightarrow XH_{01}^{0,1}$ wave to be the lowest H-wave it is necessary to have $L > 2a$. To study this situation we discuss an IDCA with geometry: $L > 2a$, $c \to L/2$ and $g \to a/2$. In this case the IDCA can be treated as a rare array with small internal grooves. Some of the possible IDCAs, namely with rectangular and triangular internal grooves (inclusions), are presented in Figs. 8(a), (b). For the IDCA parameters $L/a = 2.4$, $c/a = 1.1$ and $g/a = 0.4$, the $XH_{01}^{0,1} \leftrightarrow XH_{01}^{0,1}$ wave in the case of a rectangular groove gives $k_c a = 2.527$ and $k_c a = 2.523$ with the SDE approach and with CST, respectively. For the triangle-shaped groove CST gives $k_c a = 2.455$. The approximate formula (21) gives the value $k_c a = 2.617$. The schematic transversal field structure in the cross-section for the IDCA with the rectangular internal grooves is given in Figs. 8(b).
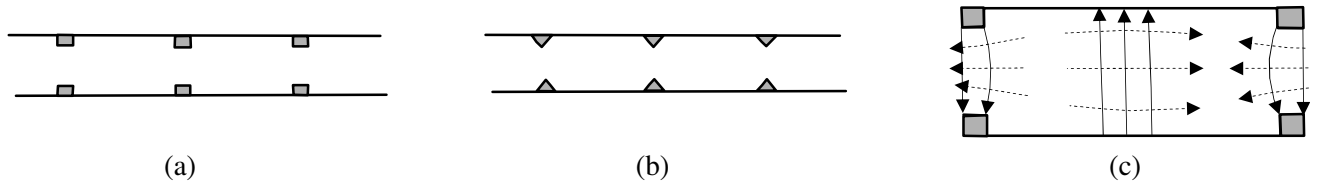

Figure 8. The IDCA with small internal (a) rectangular and (b) triangular grooves in the case $L > 2a$. (c) transversal field structure of the dominant $XH_{01}^{0,1} \leftrightarrow XH_{01}^{0,1}$-wave. E-field in solid line, H-field in dashed line.

Note that the calculation time for one point is a couple of seconds for the SDE technique, but a couple of minutes for CST.

For the *family H_z-even ($g_1 = 0$)/H_z-even ($g_2 = 0$)* the wave transition from the rectangular waveguide to the plane waveguide is presented in Fig. 9(a). For the chosen parameters the lowest
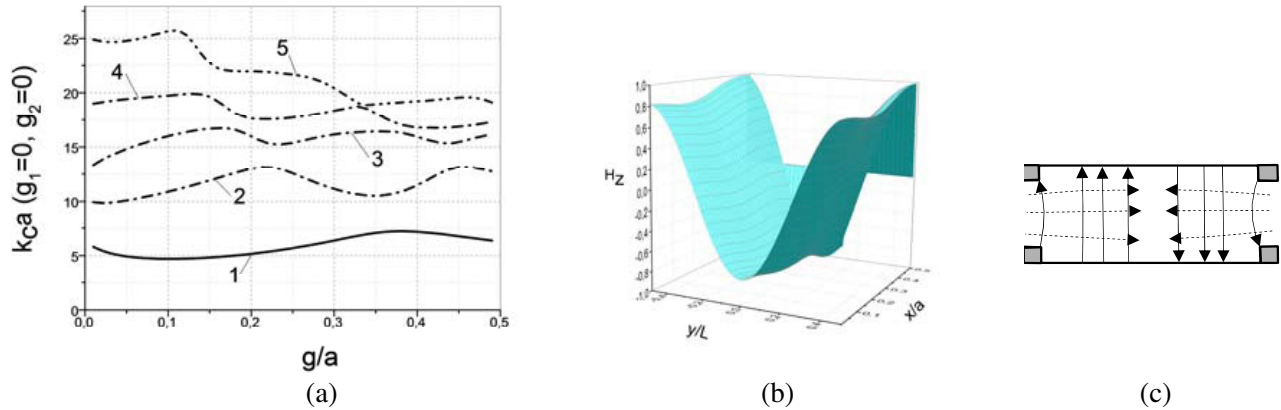
Figure 9. (a) Normalized $k_c a$ versus g/a. $c/a = 0.0484$, $L/a = 0.3876$, $L/(2c) = 4.004$. The wave transitions are: $1 — H_{20}^{0,0} \leftrightarrow H_2^{0,0}$, $2 — XH_{30}^{0,0} \leftrightarrow H_4^{0,0}$, $3 — H_{40}^{0,0} \leftrightarrow XH_{01}^{0,0}$, $4 — H_{60}^{0,0} \leftrightarrow XH_{21}^{0,0}$, $5 — H_{80}^{0,0} \leftrightarrow H_6^{0,0}$. (b) Field structure ($H_z$-component) of the $XH_{01}^{0,0}$ wave. $g/a = 0.01$. $c/a = 0.0484$, $L/a = 0.3876$, $L/(2c) = 4.004$. (c) Field structure of the $XH_{01}^{0,0}$-wave. E-field in solid line, H-field in dashed line.
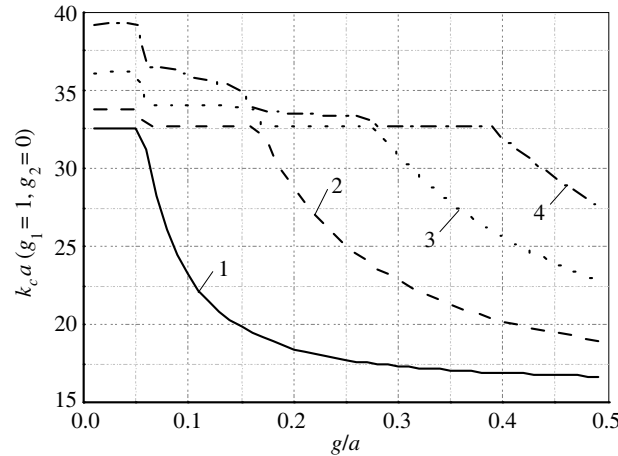

Figure 10. Normallized $k_c a$ of the IDCA versus g/a. $c/a = 0.0484$, $L/a = 0.3876$, $L/(2c) = 4.004$. The wave transitions: $1 — H_{11}^{1,1} \leftrightarrow XH_{11}^{1,1}$, $2 — H_{31}^{1,1} \leftrightarrow XH_{31}^{1,1}$, $3 — H_{51}^{1,1} \leftrightarrow XH_{51}^{1,1}$, $4 — H_{71}^{1,1} \leftrightarrow XH_{71}^{1,1}$.

wave is $H_{20}^{0,0} \leftrightarrow H_2^{0,0}$ (see curve 1). The singular wave $XH_{30}^{0,0} \leftrightarrow H_4^{0,0}$ (see curve 2) has no limit for $g/a = 0$ (does not exist) and has a limit for $g/a \to 0.5$. Also note the singular waves: $XH_{01}^{0,0}$ and $XH_{01}^{0,0}$ have no limit at $g/a \to 0.5$ and the wave $XH_{30}^{0,0}$ does not exist in the structure at $g/a = 0$. Note that in the case $g/a \to 0$ the IDCA becomes a sequence of resonators of rectangular shape coupled by slots. Therefore there are so-called slotted modes in the IDCA which dissapear when $g/a \to 0$.

It is seen from Fig. 9 that curve 3 corresponds to the singular wave $H_{40}^{0,0} \leftrightarrow XH_{01}^{0,0}$ when $g/a \to 0.5$. The field distribution of the $XH_{01}^{0,0}$ wave (H_z-component) and its schematic transversal field structure are shown in Fig. 9(b) and Fig. 9(c), respectively. This wave is similar to the previously discussed $XH_{01}^{0,1}$ wave because they both have the same critical wave number limiting value described by formula (21). However, the $XH_{01}^{0,0}$ wave belongs to another family having an electric wall in the $y = 0$ plane instead of a magnetic wall (see Fig. 1(b)). It is seen from Fig. 9(b) that the field level in region 2 prevails over the field level in region 1. A lot of coupling effects can be observed in Fig. 9(a). Due to these effects

the wave indices vary as it takes place with the transition $H_{80}^{0,0} \leftrightarrow H_6^{0,0}$.

The results for the *family H_z-odd $(g_1 = 1)/H_z$-odd $(g_2 = 1)$* are available in Fig. 10. It is seen that the regular waves of the rectangular waveguide transform to the singular waves, which do not exist in the plane waveguide. The H_z field of the $H_{11}^{1,1} \leftrightarrow XH_{11}^{1,1}$ wave is similar to the H_z field of the wave $XH_{01}^{0,1} \leftrightarrow XH_{01}^{0,1}$ and $H_{40}^{0,0} \leftrightarrow XH_{01}^{0,0}$ in the sense that it is mostly concentrated in the region 2. The normalized critical number of the $H_{11}^{1,1} \leftrightarrow XH_{11}^{1,1}$-wave at $g/a \to 0.5$ can be obtained using the formula (20) with $p = 1$, $s = 1$. For the chosen value $L/a = 0.3876$ the normalized critical wave numbers of the $XH_{11}^{1,1}$, $XH_{01}^{0,1}$, and $XH_{01}^{0,0}$ waves in the case $g/a \to 0.5$ are close to each other, namely: $k_c a = 16.51$ and $k_c a = 16.21$ (this is the same for the $XH_{01}^{0,1}$ and $XH_{01}^{0,0}$ waves), respectively.

5. CONCLUSION

In this paper the fast H-waves which propagate across an infinite double comb array have been studied. A rigorous SDE approach combined with a Galerkin scheme in which the basis functions explicitly satisfy the edge condition at the rectangular edge were used. The approach prevails over others like FEM and FDTD since it is faster and considerably more stable. Four independent wave families have been considered, and a terminology of regular and singular waves was introduced. It was shown that there are a lot of mode coupling effects in the IDCA. It was also shown that the lowest singular wave of the IDCA with small grooves has a critical wavelength equal to the IDCA period, which means that for the H-wave in the plane waveguide with periodical inclusions it can be larger than $2a$, where a is the transverse size of the plane waveguide. This was demonstrated for the plane waveguide with rectangular and triangular internal grooves. Therefore singular waves exist in an IDCA with grooves of arbitrary shapes. The results can be used in the design of diffraction radiation oscillators.

REFERENCES

1. Srivastava, V., "THz vacuum microelectronic devices," *J. Phys. Conf. Ser.*, Vol. 114, No. 1, 1–10, 2008.
2. Ives, V. R. L., "Microfabrication of high-frequency vacuum elctron devices," *IEEE Trans. Plasma Sci.*, Vol. 32, No. 3, 1277–1291, 2004.
3. Hou, Y., J. Xu, H.-R. Yin, Y.-Y. Wei, L.-N. Yue, G. Zhao, and Y.-B. Gong, "Equivalent circuit analysis of ridge-loaded folded-waveguide slow-wave structures for millimeter-wave travelling-wave tubes," *Progress In Electromagnetics Research*, Vol. 129, 215–229, 2012.
4. Hou, Y., J. Xu, S. Wang, Z.-G. Lu, Y.-Y. Wei, and Y.-B. Gong, "Study of high efficiency novel folded waveguide traveling-wave tube with sheet electron beam," *Progress In Electromagnetics Research*, Vol. 141, 431–441, 2013.
5. Liu, Y., J. Xu, Y.-Y. Wei, X. Xu, F. Shen, M. Huang, T. Tang, W.-X. Wang, Y.-B. Gong, and J. Feng, "Design of a V-band high-power sheet-beam coupled-cavity traveling-wave tube," *Progress In Electromagnetics Research*, Vol. 123, 31–45, 2012.
6. Kesari, V. and J. P. Keshari, "Analysis of a circular waveguide loaded with dielectric and metal discs," *Progress In Electromagnetics Research*, Vol. 111, 253–269, 2011.
7. Liu, S., J. Chen, S. Yu, et al., "The study of diffraction radiation oscillation," *International Journal of Infrared and Millimeter Waves*, Vol. 8, No. 8, 885–900, 1987.
8. Korneenkov, V. K., V. S. Miroshnichenko, and A. A. Shmat'ko, "Output characteristics of a diffraction radiation generator in the autonomous and nonautonomous modes," *Radiophysics and Quantum Electronics*, Vol. 34, No. 3, 251–257, 1991.
9. Belous, O. I., A. I. Fisun, A. A. Kirilenko, et al., "Research on orotron oscillator with dispersive open resonant system," *International Journal of Infrared and Millimeter Waves*, Vol. 18, No. 2, 445–461, 1997,

10. Kovalyov, I. O. and V. S. Miroshnichenko, "Frequency tuning range of diffraction radiation oscillator with periodical double comb," *Telecommunication and Radio Engineering*, Vol. 75, No. 14, 1299–1312, 2016.

11. Zargano, G. F., V. P. Lyapin, V. S. Mikhalevskiy, et al., *Complex Section Waveguides*, Radio I Svyaz, Moscow, 1986.

12. Svezhentsev, A. Ye., "Full-wave, edge-accounting calculation of losses in rectangular-groove waveguides," *Microwave and Optical Technology Letters*, Vol. 10, No. 1, 52–56, 1995.

13. Svezhentsev, A. Ye., "Full wave edge accounting analysis of waves in infinite array of stub-loaded rectangular waveguides," *International Journal of Infrared and Millimeter Waves*, Vol. 29, No. 8, 724–740, 2008.

14. Rozhnev, A. G., N. M. Ryskin, T. A. Karetnikova, G. V. Torgashev, N. I. Sinitsyn, P. D. Shalayev, and A. A. Burtsev, "Studying characteristics of the slow-wave system of the traveling-wave tube with a sheet electron beam," *Radiophysics and Quantum Electronics*, Vol. 56, No. 1, 8–9, 2014.

15. Svezhentsev, A. Ye., "Waves in an infinite array of groove waveguides," *International Conference on Mathematical Methods in Electromagnetic Theory*, CD-ROM, Kharkov, Ukraine, 2016.

16. Abramowitz, M. and I. A. Stegun, *Handbook of Mathematical Functions*, Dover, New York, 1971.

17. Melezhik, P. N., A. Y. Poyedinchuk, Y. A. Tuchkin, and V. P. Shestopalov, "Analytical nature of the vibrational mode-coupling phenomenon," *Dokl. Akad. Nauk SSSR*, Vol. 300, No. 6, 1356–1359, 1988.

18. Svezhentsev, A., "Special points of dispersion equations of metal-dielectric cylindrical waveguides," *Dokl. Akad. Nauk URSR*, No. 4, 82–87, 1994.

19. Yakovlev, A. B. and G. W. Hanson, "Analysis of mode coupling on guided wave structures using Morse critical points," *IEEE Trans. Micr. Theory and Tech.*, Vol. 46, 966–974, Jul. 1998.